ACS APPLIED MATERIALS & INTERFACES

www.acsami.org Research Article

# Magnetism-Actuated Superhydrophobic Flexible Microclaw: From Spatial Microdroplet Maneuvering to Cross-Species Control

Yahui Su, Xinran Fan, Suwan Zhu,* Zhicheng Li, Yucheng Bian, Chuanzong Li, Yiyuan Zhang, Lin Liu, Yanlei Hu, Jiawen Li, and Dong Wu*

Cite This: ACS Appl. Mater. Interfaces 2021, 13, 35165−35172 Read Online

ACCESS | Metrics & More | Article Recommendations | Supporting Information

**ABSTRACT:** The flexible maneuvering of microliter liquid droplets is significant in both fundamental science and practical applications. However, most current strategies are limited to the rigid locomotion on confined geographies platforms, which greatly hinder their practical uses. Here, we propose a magnetism-actuated superhydrophobic flexible microclaw (MSFM) with hierarchical structures for water droplet manipulation. By virtue of precise femtosecond laser patterning on magnetism-responsive poly(dimethylsiloxane) (PDMS) films doped with carbonyl iron powder, this MSFM without chemical contamination exhibits powerful spatial droplet maneuvering advantages with fast response (<100 ms) and lossless water transport (~50 cycles) in air. We further performed quantitative analysis of diverse experimental parameters including petal number, length, width, and iron element proportion in MSFM impacting the applicable maneuvering volumes. By coupling the advantages of spatial maneuverability and fast response into this versatile platform, typical unique applications are demonstrated such as programmable coalescence of droplets, collecting debris via droplets, tiny solid manipulation in aqueous severe environments, and harmless living creature control. We envision that this versatile MSFM should provide great potential for applications in microfluidics and cross-species robotics.

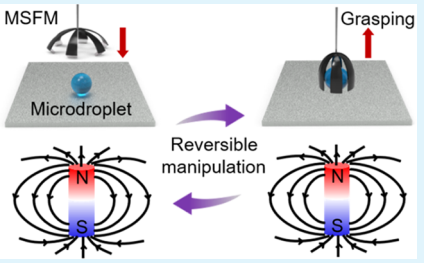


**KEYWORDS:** *droplet manipulation, laser fabrication, flexible actuator, magnetism-responsive materials, microclaw, cross-species control*

## 1. INTRODUCTION

In the past few decades, the demand for manipulation of water droplets has become a hot topic in diverse research fields such as water collection/transport,[1,2] oil−water separation,[3,4] chemical microreactions,[5,6] and bioengineering.[7,8] Generally, the main procedure of droplet manipulation includes capture, storage, and transport of droplets. Most recent microdroplet manipulation strategies rely on the assistance of specific functional surfaces in realizing droplet on-ground locomotion, which can be typically classified into superwetting surfaces[9,10] and lubricant-infused surfaces (termed SLIPSs or LISs).[11,12] Particularly, based on the driving forces linking wetting force and Laplace gradient from the specially designed geographies on the superwetting surfaces, the unidirectional locomotion of water droplets is achieved. For instance, Chen et al. fabricated superwettable microspine chips and realized the directional transportation of the droplets.[13] Jiang et al. prepared a kind of underliquid dual superlyophobic surfaces in response to external environments, which showed efficient oil and water separation performance.[14] Recently, inspired by pitcher plants in nature, another kind of emerging functional surface, termed lubricant-infused surface, has been subsequently developed for droplet manipulation that relies on its exceptional capabilities of extremely low contact angle hysteresis (<5°) and excellent repellency to foreign liquids.[15,16] For example, Zhang et al. fabricated a kind of anisotropic microgrooved organogel surfaces that could easily transport water droplets along the direction parallel to the grooves when tilted.[17] Jiang et al. prepared an anisotropic covalently grafted slippery surface with excellent anisotropic sliding behaviors toward different droplets and bubbles under water.[18]

In spite of the advantages of low cost and favorable customizability in current manipulation approaches, several obvious shortages arise subsequently: (1) Most of the current strategies are limited to rigid on-ground locomotion on the confined territories of platforms, which greatly hinder their spatial uses. For instance, droplets could only passively maneuver along the direction of Laplace pressure difference or wetting gradient on superwetting surfaces.[13,19,20] Despite the newly reported active droplet control strategies via external stimuli (e.g., electric, magnetic, light, and heat), the paths of droplet movement are still limited on the confined platform without spatial operability.[21−28] (2) To date, the current approaches utilizing functional surfaces mainly focus on the achievement of droplet manipulation itself, for which the

Received: May 17, 2021
Accepted: July 5, 2021
Published: July 13, 2021

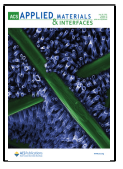






https://doi.org/10.1021/acsami.1c09142
ACS Appl. Mater. Interfaces 2021, 13, 35165−35172

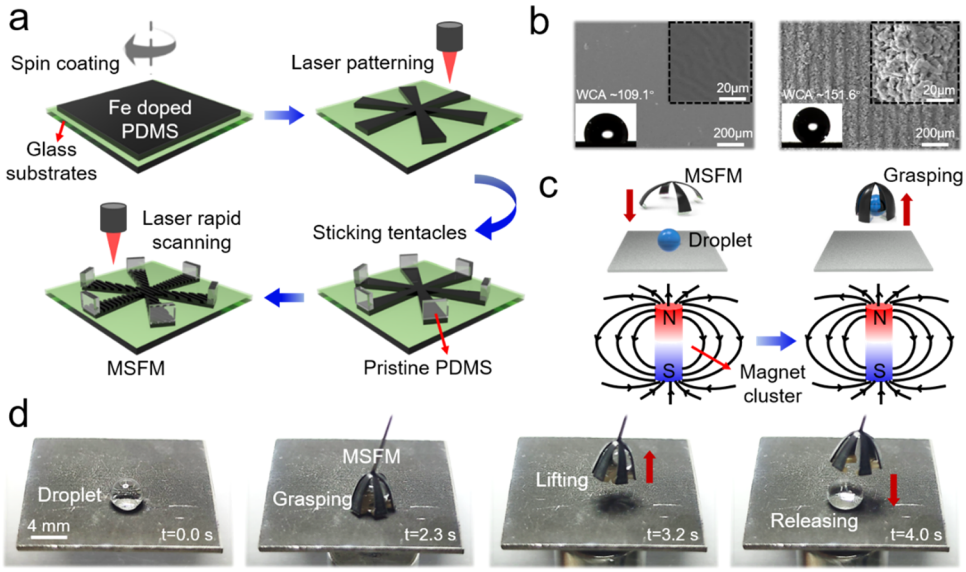


**Figure 1.** Schematic fabrication of MSFM and the grasping/releasing process toward liquid microdroplets. (a) MSFM is fabricated via the combination of precise femtosecond laser patterning and physical adhesion on PDMS. (b) SEM images of PDMS elastic films doped with the mass ratio of carbonyl iron powder to PDMS of 0.5. The WCAs are ∼109.1 and 151.6° on the surface of the smooth main arm (left) and the laser-textured main arm (right), respectively. (c) Schematic demonstration and (d) sequential snapshots of the grasping/releasing switch of microdroplets utilizing MSFM.

versatile cross-species manipulation functions are rarely exploited. In this connection, it is highly desirable for developing a new way of manipulating microdroplets that is capable of spatial maneuver flexibility and cross-species control.

Herein, we report a hybrid strategy that incorporates the good characteristics of superwetting interfaces to spatially flexible stimuli-responsive manipulators, which can readily achieve spatial transport of microdroplets by proposing a kind of magnetism-actuated laser-patterned flexible multifunctional microclaw (MSFM) with hierarchical superhydrophobic structures. Relying on the precise femtosecond laser patterning technology, the magnetism-responsive poly(dimethylsiloxane) (PDMS) film doped with carbonyl iron powder (CIP) could be precisely tailored into a petal-like microclaw, exhibiting favorable droplet control abilities with fast response (<100 ms) and lossless transport (∼50 cycles) in air. We further investigated the underlying mechanism as well as the impact of diverse experimental parameters on applicable droplet volume, including petal number, length, width, and iron element proportion in MSFM. Based on this powerful platform, typical unique cross-species control is demonstrated for potential applications including programmable coalescence of droplets, collecting debris via droplets, tiny solids manipulation in harsh aqueous solutions, and harmless control of living creatures. This versatile platform should provide new insights into microfluidics and other related applications.

## 2. RESULT AND DISCUSSION

The MSFM was fabricated using precise femtosecond laser patterning technology on the magnetism-responsive PDMS films doped with magnetic particles (Figures S1 and S2). The schematic fabrication was divided into three steps, as shown in Figure 1a. First, the elastic PDMS film (thickness ∼220 μm) was doped with carbonyl iron powder (CIP) and then patterned into petal shape by femtosecond laser ablation (mean power 300 mW, scanning speed 1 mm/s). Second, the tentacles with a height of 1 mm (pristine PDMS film, thickness ∼500 μm) were fast scanned line-by-line under laser irradiation at the speed of 10 mm/s (mean power 300 mW, scanning spacing 50 μm). The laser-ablated tentacles were then stuck on the end of the petals by liquid PDMS/curing agent mixture and cured on the heating plate for 0.5 h at the temperature of 100 °C. We chose pristine PDMS as the tentacle material because CIP-doped tentacles would also deform when closed to the magnetic field, resulting in the capturing/releasing failure (Figure S3). Third, the as-prepared samples were fast scanned line-by-line in the same laser irradiation conditions. The surface morphology and wettability were characterized before/after laser fast scanning (Figure 1b). It can be observed that the water contact angle (WCA) on the smooth Fe-doped PDMS was measured to be ∼109.1°. After laser fast scanning, a series of periodic microgrooves were formed on the MSFM surface along with numerous micro/nanomastoids according to scanning electron microscopy (SEM) images. Meanwhile, the WCA significantly increased to ∼151.6° with enhanced surface roughness.

The hierarchical structures on the MSFM were further visualized by higher resolution SEM images, in which periodic micron-sized groove and scattered nanoscale mastoid could be clearly observed on both the tentacles and the main arms (Figure S4). In addition, although the laser scanning process was the same, the micro/nanostructures on the two materials showed a slight difference: the average size of micro/nanoparticles on the CIP-doped PDMS main arms was a bit larger than those on the pristine PDMS tentacles. It should be emphasized that the hierarchical structures of the protruding tentacles and the main arms endow MSFM with the capability of grasping/releasing microdroplets in a lossless manner, which is vividly demonstrated in Figure 1c,d. Unless otherwise specified, deionized water droplets were used throughout the experiments. We used a remote fashion by organizing five NdFeB cylindrical magnets (both diameter and thickness were 10 mm) into a cluster and placed them under the


https://doi.org/10.1021/acsami.1c09142
ACS Appl. Mater. Interfaces 2021, 13, 35165−35172

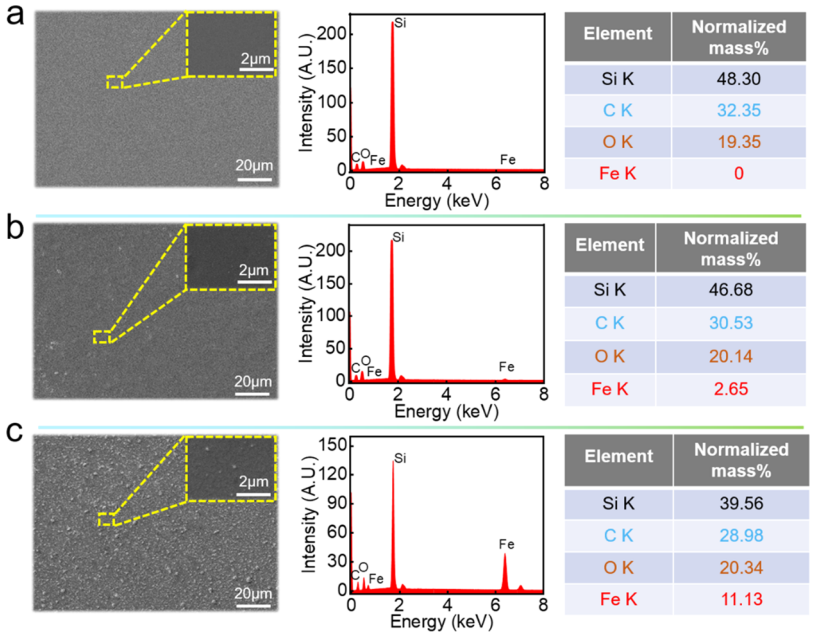


**Figure 2.** SEM images of and EDS analysis of the MSFM surfaces doped with different mass ratios of carbonyl iron powder to PDMS: (a) 0, (b) 0.5, and (c) 1.

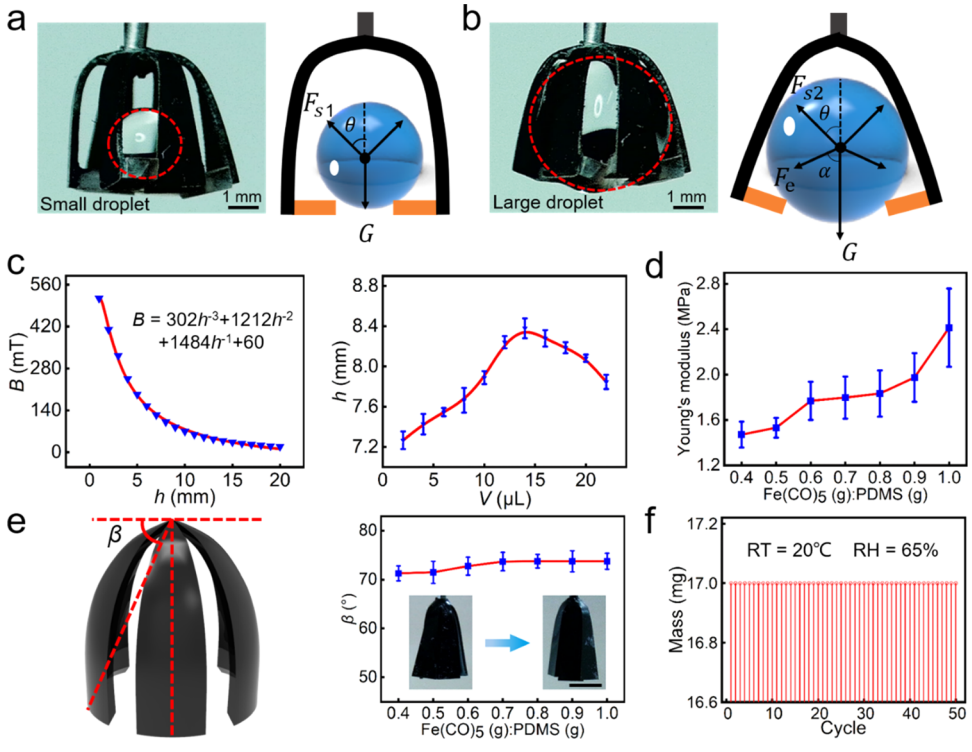


**Figure 3.** Droplet control mechanism and properties of MSFM under magnetism stimuli. (a), (b) Force analysis on the static droplets captured by MSFM in two distinct droplet volumes. (c) Left: Relation of MFD $B$ and the height $h$ between MSFM and magnet cluster. Right: Relation between maximum lifting height and targeted droplet volume in droplet control. The MFD was measured near the north pole of the magnet cluster. (d) Relation between Young's modulus and MRCP. (e) Relation between deformation amplitude and MRCP. Scale bar is 2 mm. (f) Fifty-cycle repeatability experiment of the droplet grasping/releasing indicates the lossless droplet control.

superhydrophobic aluminum substrate. The magnetic flux density (MFD) was measured through a high-precision Gauss meter (Figure S5). Here, both the MSFM and magnet cluster were actuated and guided manually to ensure their synchronous movement. Once the MSFM gets close to the upward side of the droplets, the decurved magnetism-responsive microclaw would finally close and capture the droplets as long as the MFD is large enough, which could be easily tuned by the height between the microdroplet and the magnet cluster.

We further characterized the surface morphology and chemical element components on the main arm of MSFM in



https://doi.org/10.1021/acsami.1c09142
ACS Appl. Mater. Interfaces 2021, 13, 35165−35172

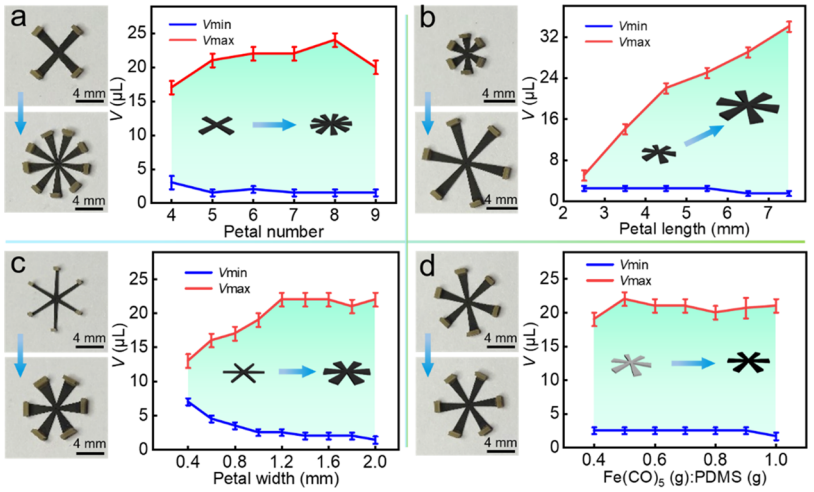


**Figure 4.** Quantitative investigation for the impact of diverse experimental parameters on the applicable volume range during droplet control via MSFM, including (a) petal number, (b) petal length, (c) petal width, and (d) mass ratio of carbonyl iron powder to PDMS.

different mass ratios of carbonyl iron powder to PDMS (MRCP) = 0, 0.5, and 1, which are crucial for microdroplet manipulation performance. As shown in Figure 2, an increased MRCP resulted in enhanced surface roughness, exhibiting more sporadic microparticles on the surface. In addition, X-ray spectroscopy (EDS) revealed the detailed proportions (normalized mass ratio) of the elements Si, C, O, and Fe on each MSFM surface. It can be found that the proportion of element Fe significantly increased from 0 to 11.13% as MRCP increased from 0 to 1. As a consequence, the proportions of elements Si, C, and O decreased drastically from 48.30, 32.35, and 19.35% to 39.5, 28.98, and 20.34%, respectively.

The basic mechanism for the spatial microdroplet capturing/releasing process of MSFM under magnetic field stimuli was investigated. Figure 3a,b shows the photographic images and the force analysis for static droplet-grasping states using MSFM in different water volumes (see also Movie S1), where typical petal number, length, width, and MRCP were set as 6, 4.5 mm, 1.4 mm, and 0.5, respectively. For a static small droplet captured by MSFM (Figure 3a), only the bottom of the droplet contacted the upper surfaces on the tentacles. In this situation, only two kinds of forces are exerted on the water droplet, which are gravitational force $G$ of the droplet and the support force $F_{s1}$ from a single tentacle of MSFM. The component force of the total $F_{s1}$ along the opposite direction of $G$ should be equal to $G$

$$6F_{s1}\cos\theta = G \tag{1}$$

where $\theta$ is the included angle between the direction of $F_{s1}$ and the opposite direction of $G$. As for the state of a large droplet captured by MSFM, due to the limited lateral width inside a closed MSFM, the large droplet contacted with both the upper surfaces on the tentacles and the sidewalls on the main arms, as definitely shown in the photographic image in Figure 3b. In this case, there are three kinds of forces acting on the large droplet, which are the droplet's gravitational force $G$, the support force $F_{s2}$ from a single tentacle, and the extrusion force $F_e$ from a single main arm of MSFM. At this point, the component force of the total $F_{s2}$ in the opposite direction of $G$ should be equal to the resultant force consisting of $G$ and the component of the total $F_e$ along the direction of $G$

$$6F_{s2}\cos\theta = G + 6F_e\cos\alpha \tag{2}$$

where $\alpha$ is the inclined angle between the direction of $F_e$ and the direction of $G$. As mentioned earlier, a large enough MFD would result in the bending of MSFM along the magnetic field direction. Once the support forces are large enough, the microdroplet could be lifted upward. On the contrary, the releasing process of a microdroplet is a reverse process compared to the grasping process, which can be achieved by elevating the droplet height to decrease the MFD below an unfolding threshold of a closed MSFM.

It should be noted that the trigger of the grasping/releasing switch, MFD, could be facilely adjusted by the height between the magnetic cluster and the MSFM. Figure 3c shows the variation of MFD with different heights between the NdFeB magnet cluster and the center of an MSFM (left) and the relation between the maximum lifting height and the targeted droplet volume (right). It can be clearly seen that the mean MFD $B$ decreased dramatically with an increase in the height $h$ between the magnet cluster and the MSFM and followed the relation $B = 302h^{-3} + 1212h^{-2} + 1484h^{-1} + 60$, which indicated that the droplet-grasping state could only sustain within a confined height range for the MSFM. The maximum lifting height for a droplet increased with the droplet volume $V$ and reached an extrema of ~8.4 mm at $V \approx 14$ $\mu$L, and the corresponding MFD was measured as ~100.4 mT. Interestingly, once the droplet volume $V$ exceeded 14 $\mu$L, the maximum lifting height showed a declining trend with an increase in $V$. This phenomenon could be interpreted by the above-mentioned force analysis. When the droplet volume is relatively small, the microdroplet does not contact the main arms of MFPM and only suffers from two forces $G$ and $F_s$. When the MSFM is slightly elevated away from the substrate, the smaller droplet is more likely to escape from the gaps of the MSFM driven by $G$. As the droplet volume/diameter continues to increase over a threshold, it will eventually contact and be squeezed by the main arms, followed by triggering the releasing process of the droplet. Consequently, an increasing droplet volume intensifies the "squeezing effect" by assuming that the height $h$ is constant.

We further quantitatively discussed the effect of MRCP on the mechanical property and deformation amplitude of the MSFM arms. We used a typical six-petal MSFM (petal width = 1.4 mm, length = 4.5 mm) at a 5 mm minimum height above a five-magnet cluster ($B \approx 190$ mT). Figure 3d indicates that


https://doi.org/10.1021/acsami.1c09142
ACS Appl. Mater. Interfaces 2021, 13, 35165−35172

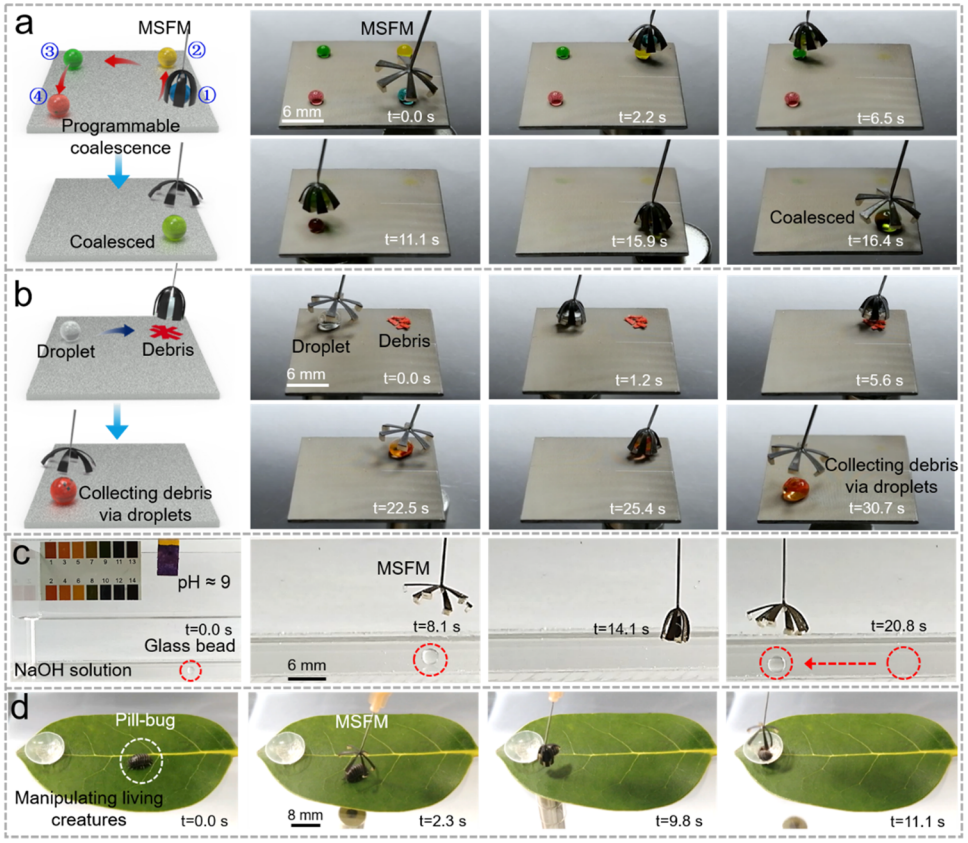


**Figure 5.** Typical cross-species control applications through MSFM are vividly demonstrated including (a) programmable coalescence of droplets, (b) collecting debris via droplets, (c) manipulating solid glass beads in aqueous NaOH solution, and (d) harmless control of living creatures.

Young's modulus increased sharply from approximately 1.5−2.4 MPa as the MRCP increased from 0.4 to 1. However, no notable difference was observed in the magnetism-induced deformation on the main arms in different MRCPs (Figure 3e). Here, the deformation amplitude was defined as the decurved angle $\beta$ deviating from the horizontal by the magnetic force. The reliability of the MSFM during repeated grasping/releasing transition was also investigated. A 50 cycle repeatability experiment for grasping/releasing a 17 $\mu$L deionized water droplet is shown in Figure 3f. We adopted the above-mentioned typical six-petal MSFM with an MRCP of 0.5. To better suppress the water evaporation during its mass measurement, the transport and measurement experiments were performed in a small sealed acrylic box (RT = 20 °C, RH = 65%). In a contrast experiment, a static 17 $\mu$L droplet was placed on the sealed box, and its mass reading was recorded every 1 min by a high-accuracy electronic balance. As evidenced by Figure S6, the water evaporation was negligible within the 10 min measurement. After each independent grasping/releasing period, the mass of the droplet was recorded. During the 50 repeated cycles in 10 min, the droplet mass remained almost the same value at ∼17 mg, which firmly suggested the excellent ability of lossless manipulation of microdroplets.

Next, a series of key metrics for the microdroplet manipulation performance of MSFM were quantified, including petal number, length, width, and MRCP. We focused on the impact of these experimental parameters on the microdroplet loading capacity (MLC) of the MSFM, i.e., the applicable volume range (green areas in Figure 4). Figure 4a shows the influence of petal number on MLC. When the petal number increased from 4 to 9, the minimum MLC did not change significantly (∼2 $\mu$L) and the maximum MLC reached an extrema of ∼24 $\mu$L at the petal number of 8. The experimental results indicate that grasping smaller microdroplets is insensitive to the petal number. This is probably due to the fact that the smaller droplets could easily slip away from the gaps between each main arm relative to the droplet diameter. As the petal number increases to 9, the closing process of MFPM is restricted by each adjacent tentacle, which also restricts the degree of closure and facilitates the droplet escape. On the contrary, the larger droplets could be firmly clamped and hardly slip away with an increased number of main arms for MSFM (Figure 3b). Similar results were found when the petal length increased (Figure 4b). The minimum MLC change slightly (∼2 $\mu$L) and the maximum MLC increased significantly from ∼5 to ∼35 $\mu$L as the petal length increased from 2.5 to 7.5 mm. Because the longer main arm could provide extra contact areas and internal space, which allows for manipulating droplets with greater diameters.

The impact of petal width on MLC for MSFM was investigated and is shown in Figure 4c. Interestingly, the minimum MLC decreased significantly from 7 to 1 $\mu$L with the elevated petal width, whereas the maximum MLC increased from 14 to 23 $\mu$L. This could be probably attributed to the fact that wider main arms could decrease the gap between each adjacent main arm and provide larger lateral contact areas, which further broaden the applicable volume range of microdroplets for MSFM. In addition, the relation between MLC and MRCP is presented in Figure 4d. It can be observed that the minimum MLC was insensitive to MRCP (∼2 $\mu$L). The upper limit of MLC increased with the elevated MRCP


https://doi.org/10.1021/acsami.1c09142
ACS Appl. Mater. Interfaces 2021, 13, 35165−35172

and rapidly reached an extrema of ∼22 μL at MRCP of 0.5, which indicated that the optimal magnetism-responsive performance was achieved in this system.

Finally, by coupling the major merits of spatial maneuverability and fast response to this versatile platform, we demonstrated typical unique cross-species control for potential applications including programmable coalescence of droplets, collecting debris via droplets, tiny solid control in harsh aqueous solutions, and even harmless living creature maneuvering (Figure 5), which are otherwise challenging for conventional microdroplet manipulation strategies solely relying on superwetting and LIS platforms. As shown in Figure 5a, the programmable coalescence of four colored microdroplets was successfully achieved by a typical MSFM within 6.5 s, showing a high-efficiency programmable droplet control capability (Movie S2). Here, the deionized water droplets were stained into different colors by water-soluble food coloring for better observation. Different from the recently reported water droplet manipulation relying on anisotropic adhesion between water and hydrophobic−superhydrophobic patterned surfaces or liquid-infused surfaces, our flexible microclaw exhibits not only excellent lossless droplet transport but also cross-species sample control.[29,30] Accordingly, collecting debris via droplets was further demonstrated (Figure 5b). The solid debris was collected and transported sequentially by the interfacial adhesion between the paper scraps and a 17 μL droplet clamped by a typical MSFM beforehand (Movie S3).

Our MSFM system could also be deployed in severe environments such as alkaline and acidic aqueous solutions (Movie S4 and Figure S7). As a paradigm, Figure 5c indicates that the MSFM could function well in manipulating solid glass beads in the NaOH solution. To investigate the chemical and wettability stability for droplet control in the air after the underwater action, we performed an additional experiment. As proved by Movie S5, the microclaw could still effectively capture/release water droplets in the air after manipulating items in alkaline solutions, which indicated its favorable durability in different ambient surroundings. The excellent properties of softness, flexibility, and biocompatibility have also endowed the MSFM with the harmless manipulation of living creatures (Figure 5d). Owing to the fast response of MSFM under magnetic field stimuli (<100 ms), a crawling pill bug on a green leaf could be harmlessly captured and subsequently transported (Movie S6).

## 3. CONCLUSIONS

We developed a kind of microdroplet maneuvering platform MSFM that consists of patterned PDMS elastic microclaw with a hierarchical structure. By doping carbonyl iron power into the main arms of the microclaw, the magnetism-responsive platform is capable of realizing spatial control of droplets with such advantages as fast response (<100 ms) and lossless water transport (∼50 cycles) in the air. We systematically investigated the grasping/releasing mechanism and the impact of petal number, length, width, and mass ratio of carbonyl iron powder on the droplet loading range of MSFM. We emphasize the cross-species maneuvering capability of this powerful system, which is further embodied in a series of demonstrations including programmable coalescence of droplets, collecting debris via droplets, manipulating tiny solids in harsh aqueous solutions, and harmless manipulation of living creatures. This versatile MSFM should open up more possibilities in many application fields such as microfluidics and intelligent manipulators.

## 4. EXPERIMENTAL SECTION

**Materials.** The carbonyl iron powder particles (∼7 μm, ≥99% purity) were purchased from Nantong Jia Nuo Alloy Material Co., Ltd. The cylindrical NdFeB magnets with a diameter and a thickness of 10 mm used in the experiment were purchased from Shanghai Jin Cheng Mechanical & Electrical Co., Ltd. The transparent PDMS film was purchased from Hangzhou Baoerde New Material Technology Co., Ltd. The adjustable rotation speed of the spin coater was between 100 and 7000 rpm at factory settings. The typical rotational speed in sample preparation was ∼700 rpm and the rotational time was ∼10 s.

**Fabrication of the PDMS Elastic Film.** First, liquid PDMS prepolymer (Sylgard 184, Dow Corning), cross-linker, and carbonyl iron powder (CI) (10:1:5, PDMS precursor: cross-linking agent: CI, by weight) (PDMS/CI mixed solution) were dropped in a beaker; then, the PDMS/CI mixed solution was stirred with a glass rod for 10 min to form a homogeneous mixture. Second, 0.565 g of the mixture was put on a glass substrate, spin-coated by a homogenizer (700 rpm, 10 s), then made to stand for 20 min to degas. Finally, the PDMS elastic film was obtained after curing for 50 min at 90 °C in an electric oven.

**Femtosecond Laser Processing of MSFM.** A Ti: sapphire femtosecond laser system (Legend-Elite-1K-HE, Coherent) was employed to cut the PDMS elastic film into a petal shape and to scan the surface of microclaw after sticking tentacles. The laser duration, repetition rate, and center wavelength were 104 fs, 1 kHz, and 800 nm, respectively. The laser scanning path was guided by a galvanometer scanner.

**Characterization.** Surface morphologies of the samples were observed by a secondary electron SEM (Zeiss EVO18) with an accelerating voltage at 20 kV. Chemical component analysis was measured through EDS (Bruker XFlash 6130). The magnetic flux density was measured by a digital Gauss meter (HM-100, Huaming Instrument Co., Ltd., China). WCA measurements were carried out by an optical contact angle meter (CA100C, Innuo, China) at ambient temperature using a fixed water volume of 2 μL. The droplet mass measurements were performed on a high-accuracy electronic balance with a minimum accuracy of 0.1 mg. Young's modulus was measured by a solids analyzer (RSA-G2, TA Instruments) at a fixed tensile speed of 25 μm/s.

## ■ ASSOCIATED CONTENT

### Supporting Information

The Supporting Information is available free of charge at https://pubs.acs.org/doi/10.1021/acsami.1c09142.

Schematic of the chemical synthesis of the magnetism-responsive PDMS films, fs-laser precise patterning process of MSFM, shape deformation of the tentacles and the main arms under magnetic field stimuli, hierarchical structures consisting of microgrooves and nanomastoid on tentacles and main arms, specific measurement method for magnetic flux density, mass variation of a 17 μL droplet in the sealed acrylic box in 10 min, and demonstration of manipulating solid glass beads in aqueous HCl solution (PDF)

Grasping and releasing of small and large droplets (AVI)

Programmable coalescence of droplets (AVI)

Collecting debris via droplets (AVI)

Manipulating solid glass beads in NaOH and HCl solutions (AVI)

Favorable durability in different ambient surroundings (AVI)

Harmless manipulation of living creature (AVI)



https://doi.org/10.1021/acsami.1c09142
ACS Appl. Mater. Interfaces 2021, 13, 35165−35172

## AUTHOR INFORMATION


### Corresponding Authors

**Suwan Zhu** − *CAS Key Laboratory of Mechanical Behavior and Design of Materials, Key Laboratory of Precision Scientific Instrumentation of Anhui Higher Education Institutes, Department of Precision Machinery and Precision Instrumentation, University of Science and Technology of China, Hefei 230026, China;* orcid.org/0000-0001-9881-5694; Email: suwanzhu@ustc.edu.cn

**Dong Wu** − *CAS Key Laboratory of Mechanical Behavior and Design of Materials, Key Laboratory of Precision Scientific Instrumentation of Anhui Higher Education Institutes, Department of Precision Machinery and Precision Instrumentation, University of Science and Technology of China, Hefei 230026, China;* orcid.org/0000-0003-0623-1515; Email: dongwu@ustc.edu.cn

### Authors

**Yahui Su** − *Information Materials and Intelligent Sensing Laboratory of Anhui Province, School of Electronics and Information Engineering, Anhui University, Hefei 230039, China*

**Xinran Fan** − *Information Materials and Intelligent Sensing Laboratory of Anhui Province, School of Electronics and Information Engineering, Anhui University, Hefei 230039, China*

**Zhicheng Li** − *Information Materials and Intelligent Sensing Laboratory of Anhui Province, School of Electronics and Information Engineering, Anhui University, Hefei 230039, China*

**Yucheng Bian** − *CAS Key Laboratory of Mechanical Behavior and Design of Materials, Key Laboratory of Precision Scientific Instrumentation of Anhui Higher Education Institutes, Department of Precision Machinery and Precision Instrumentation, University of Science and Technology of China, Hefei 230026, China*

**Chuanzong Li** − *School of Instrument Science and Opto-Electronics Engineering, Hefei University of Technology, Hefei 230009, China*

**Yiyuan Zhang** − *CAS Key Laboratory of Mechanical Behavior and Design of Materials, Key Laboratory of Precision Scientific Instrumentation of Anhui Higher Education Institutes, Department of Precision Machinery and Precision Instrumentation, University of Science and Technology of China, Hefei 230026, China;* orcid.org/0000-0002-0393-2597

**Lin Liu** − *School of Instrument Science and Opto-Electronics Engineering, Hefei University of Technology, Hefei 230009, China*

**Yanlei Hu** − *CAS Key Laboratory of Mechanical Behavior and Design of Materials, Key Laboratory of Precision Scientific Instrumentation of Anhui Higher Education Institutes, Department of Precision Machinery and Precision Instrumentation, University of Science and Technology of China, Hefei 230026, China;* orcid.org/0000-0003-1964-0043

**Jiawen Li** − *CAS Key Laboratory of Mechanical Behavior and Design of Materials, Key Laboratory of Precision Scientific Instrumentation of Anhui Higher Education Institutes, Department of Precision Machinery and Precision Instrumentation, University of Science and Technology of China, Hefei 230026, China;* orcid.org/0000-0003-3950-6212

Complete contact information is available at: https://pubs.acs.org/10.1021/acsami.1c09142


### Author Contributions

Y.S. and X.F. performed the experiment. Z.L., Y.B., C.L., and Y.Z. fabricated the samples. S.Z., X.F., and L.L. analyzed the data. S.Z., X.F., J.L., Y.H., and D.W. prepared and revised the manuscript. S.Z. and D.W. contributed the materials and experimental instruments.

### Notes

The authors declare no competing financial interest.

## ACKNOWLEDGMENTS

This work was supported by the National Natural Science Foundation of China (Nos. 51875544, 61505047, and 61805230), the Fundamental Research Funds for the Central Universities (Nos. WK2090000035, WK2480000005, WK2090090025, and JZ2017YYPY0240), the National Key R&D Program of China (2017YFB1104303), and the China Postdoctoral Science Foundation (No. 2018M642534). We acknowledge the Experimental Center of Engineering and Material Sciences at USTC for the fabrication and measurement of the samples.

## REFERENCES


(1) Liu, M. J.; Wang, S. T.; Jiang, L. Nature-inspired superwettability systems. *Nat. Rev. Mater.* **2017**, *2*, No. 17036.

(2) Nan, L.; Lai, M. Y. A.; Tang, M. Y. H.; Chan, Y. K.; Poon, L. L. M.; Shum, H. C. On-Demand Droplet Collection for Capturing Single Cells. *Small* **2020**, *16*, No. 1902889.

(3) Zheng, X.; Guo, Z. Y.; Tian, D. L.; Zhang, X. F.; Jiang, L. Electric Field Induced Switchable Wettability to Water on the Polyaniline Membrane and Oil/Water Separation. *Adv. Mater. Interfaces* **2016**, *3*, No. 1600461.

(4) Zhou, C. L.; Cheng, J.; Hou, K.; Zhao, A.; Pi, P. H.; Wen, X. F.; Xu, S. P. Superhydrophilic and underwater superoleophobic titania nanowires surface for oil repellency and oil/water separation. *Chem. Eng. J.* **2016**, *301*, 249−256.

(5) Yang, Y.; Li, X. J.; Zheng, X.; Chen, Z. Y.; Zhou, Q. F.; Chen, Y. 3D-Printed Biomimetic Super-Hydrophobic Structure for Microdroplet Manipulation and Oil/Water Separation. *Adv. Mater.* **2018**, *30*, No. 1704912.

(6) Tan, Y. L.; Hu, B. R.; Chu, Z. Y.; Wu, W. J. Bioinspired Superhydrophobic Papillae with Tunable Adhesive Force and Ultralarge Liquid Capacity for Microdroplet Manipulation. *Adv. Funct. Mater.* **2019**, *29*, No. 1900266.

(7) Zhang, Y.; Wang, T. H. Full-range Magnetic Manipulation of Droplets via Surface Energy Traps Enables Complex Bioassays. *Adv. Mater.* **2013**, *25*, 2903−2908.

(8) Gao, Z. F.; Liu, R.; Wang, J. H.; Dai, J.; Huang, W. H.; Liu, M. J.; Wang, S. T.; Xia, F.; Jiang, L. Controlling Droplet Motion on an Organogel Surface by Tuning the Chain Length of DNA and its Biosensing Application. *Chem* **2018**, *4*, 2929−2943.

(9) Dai, H. Y.; Dong, Z. C.; Jiang, L. Directional liquid dynamics of interfaces with superwettability. *Sci. Adv.* **2020**, *6*, No. eabb5528.

(10) Zhao, Z. G.; Li, C. X.; Dong, Z. C.; Yang, Y. C.; Zhang, L. H.; Zhuo, S. Y.; Zhou, X. T.; Xu, Y. C.; Jiang, L.; Liu, M. J. Adaptive Superamphiphilic Organohydrogels with Reconfigurable Surface Topography for Programming Unidirectional Liquid Transport. *Adv. Funct. Mater.* **2019**, *29*, No. 1807858.

(11) Cao, M. Y.; Guo, D. W.; Yu, C. M.; Li, K.; Liu, M. J.; Jiang, L. Water-Repellent Properties of Superhydrophobic and Lubricant-Infused "Slippery" Surfaces: A Brief Study on the Functions and Applications. *ACS Appl. Mater. Interfaces* **2016**, *8*, 3615−3623.

(12) Che, P. D.; Heng, L. P.; Jiang, L. Lubricant-Infused Anisotropic Porous Surface Design of Reduced Graphene Oxide Toward

Electrically Driven Smart Control of Conductive Droplets' Motion. *Adv. Funct. Mater.* **2017**, *27*, No. 1606199.
(13) Chen, Y. X.; Li, K.; Zhang, S. D.; Qin, L.; Deng, S. H.; Ge, L. Y.; Xu, L. P.; Ma, L. L.; Wang, S. T.; Zhang, S. J. Bioinspired Superwettable Microspine Chips with Directional Droplet Transportation for Biosensing. *ACS Nano* **2020**, *14*, 4654−4661.
(14) Zhao, Z. H.; Ning, Y. Z.; Jin, X.; Ben, S.; Zha, J. L.; Su, B.; Tian, D. L.; Liu, K. S.; Jiang, L. Molecular-Structure-Induced Under-Liquid Dual Superlyophobic Surfaces. *ACS Nano* **2020**, *14*, 14869−14877.
(15) Wong, T. S.; Kang, S. H.; Tang, S. K. Y.; Smythe, E. J.; Hatton, B. D.; Grinthal, A.; Aizenberg, J. Bioinspired self-repairing slippery surfaces with pressure-stable omniphobicity. *Nature* **2011**, *477*, 443−447.
(16) Xiang, T. F.; Zheng, S. L.; Zhang, M.; Sadig, H. R.; Li, C. Bioinspired Slippery Zinc Phosphate Coating for Sustainable Corrosion Protection. *ACS Sustainable Chem. Eng.* **2018**, *6*, 10960−10968.
(17) Zhang, P. C.; Liu, H. L.; Meng, J. X.; Yang, G.; Liu, X. L.; Wang, S. T.; Jiang, L. Grooved Organogel Surfaces towards Anisotropic Sliding of Water Droplets. *Adv. Mater.* **2014**, *26*, 3131−3135.
(18) Wang, X.; Wang, Z. B.; Heng, L. P.; Jiang, L. Stable Omniphobic Anisotropic Covalently Grafted Slippery Surfaces for Directional Transportation of Drops and Bubbles. *Adv. Funct. Mater.* **2020**, *30*, No. 1902686.
(19) Huang, S.; Yin, S. H.; Chen, F. J.; Luo, H.; Tang, Q. C.; Song, J. L. Directional transport of droplets on wettability patterns at high temperature. *Appl. Surf. Sci.* **2018**, *428*, 432−438.
(20) Yan, X.; Qin, Y. M.; Chen, F. P.; Zhao, G. L.; Sett, S.; Hoque, M. J.; Rabbi, K. F.; Zhang, X. Q.; Wang, Z.; Li, L. N.; Chen, F.; Feng, J.; Miljkovic, N. Laplace Pressure Driven Single-Droplet Jumping on Structured Surfaces. *ACS Nano* **2020**, *14*, 12796−12809.
(21) Chen, C.; Huang, Z. C.; Jiao, Y. L.; Shi, L. A.; Zhang, Y. Y.; Li, J. W.; Li, C. Z.; Lv, X. D.; Wu, S. Z.; Hu, Y. L.; Zhu, W. L.; Wu, D.; Chu, J. R.; Jiang, L. In Situ Reversible Control between Sliding and Pinning for Diverse Liquids under Ultra-low Voltage. *ACS Nano* **2019**, *13*, 5742−5752.
(22) Chen, C.; Zhou, L. L.; Shi, L. A.; Zhu, S. W.; Huang, Z. C.; Xue, C.; Li, J. W.; Hu, Y. L.; Wu, D.; Chu, J. R. Ultralow-Voltage-Driven Smart Control of Diverse Drop's Anisotropic Sliding by in Situ Switching Joule Heat on Paraffin-Infused Microgrooved Slippery Surface. *ACS Appl. Mater. Interfaces* **2020**, *12*, 1895−1904.
(23) Guo, P.; Wang, Z. B.; Heng, L. P.; Zhang, Y. Q.; Wang, X.; Jiang, L. Magnetocontrollable Droplet and Bubble Manipulation on a Stable Amphibious Slippery Gel Surface. *Adv. Funct. Mater.* **2019**, *29*, No. 1808717.
(24) Han, K. Y.; Heng, L. P.; Zhang, Y. Q.; Liu, Y.; Jiang, L. Slippery Surface Based on Photoelectric Responsive Nanoporous Composites with Optimal Wettability Region for Droplets' Multifunctional Manipulation. *Adv. Sci.* **2019**, *6*, No. 1801231.
(25) Guo, T. Q.; Che, P. D.; Heng, L. P.; Fan, L. Z.; Jiang, L. Anisotropic Slippery Surfaces: Electric-Driven Smart Control of a Drop's Slide. *Adv. Mater.* **2016**, *28*, 6999−7007.
(26) Wu, D.; Wu, S. Z.; Chen, Q. D.; Zhang, Y. L.; Yao, J.; Yao, X.; Niu, L. G.; Wang, J. N.; Jiang, L.; Sun, H. B. Curvature-Driven Reversible In Situ Switching Between Pinned and Roll-Down Superhydrophobic States for Water Droplet Transportation. *Adv. Mater.* **2011**, *23*, 545−549.
(27) Seo, J.; Lee, J. S.; Lee, K.; Kim, D.; Yang, K.; Shin, S.; Mahata, C.; Jung, H. B.; Lee, W.; Cho, S. W.; Lee, T. Switchable Water-Adhesive, Superhydrophobic Palladium-Layered Silicon Nanowires Potentiate the Angiogenic Efficacy of Human Stem Cell Spheroids. *Adv. Mater.* **2014**, *26*, 7043−7050.
(28) Yang, C.; Wu, L.; Li, G. Magnetically Responsive Superhydrophobic Surface: In Situ Reversible Switching of Water Droplet Wettability and Adhesion for Droplet Manipulation. *ACS Appl. Mater. Interfaces* **2018**, *10*, 20150−20158.
(29) Yang, X. L.; Choi, W. T.; Liu, J. Y.; Liu, X. Droplet Mechanical Hand Based on Anisotropic Water Adhesion of Hydrophobic-Superhydrophobic Patterned Surfaces. *Langmuir* **2019**, *35*, 935−942.
(30) Liu, W. J.; Luo, X.; Chen, C. H.; Jiang, G. C.; Hu, X. Y.; Zhang, H. J.; Zhong, M. L. Directional anchoring patterned liquid-infused superamphiphobic surfaces for high-throughput droplet manipulation. *Lab Chip* **2021**, *21*, 1373−1384.


https://doi.org/10.1021/acsami.1c09142
*ACS Appl. Mater. Interfaces* 2021, 13, 35165−35172